CHINESE JOURNAL OF MECHANICAL ENGINEERING
Vol. 26, No. 6, 2013

DOI: 10.3901/CJME.2013.06.1250, available online at www.springerlink.com; www.cjmenet.com; www.cjmenet.com.cn

Mechanisms of Accelerated Degradation in the Front Cells of PEMFC Stacks and Some Mitigation Strategies

LI Pengcheng[1], PEI Pucheng[2,*], HE Yongling[1], YUAN Xing[2], CHAO Pengxiang[2], and WANG Xizhong[2]

1 *School of Transportation Science and Engineering, Beihang University, Beijing 100191, China*
2 *State Key Laboratory of Automotive Safety and Energy, Tsinghua University, Beijing 100084, China*

Received September 6, 2012; revised July 29, 2013; accepted August 27, 2013

Abstract: The accelerated degradation in the front cells of a polymer electrolyte membrane fuel cell(PEMFC) stack seriously reduces the reliability and durability of the whole stack. Most researches only focus on the size and configuration of the gas intake manifold, which may lead to the maldistribution of flow and pressure. In order to find out the mechanisms of the accelerated degradation in the front cells, an extensive program of experimental and simulation work is initiated and the results are reported. It is found that after long-term lifetime tests the accelerated degradation in the front cells occurs in all three fuel cell stacks with different flow-fields under the U-type feed configuration. Compared with the rear cells of the stack, the voltage of the front cells is much lower at the same current densities and the membrane electrode assembly(MEA) has smaller active area, more catalyst particle agglomeration and higher ohmic impedance. For further investigation, a series of three dimensional isothermal numerical models are built to investigate the degradation mechanisms based on the experimental data. The simulation results reveal that the dry working condition of the membrane and the effect of high-speed gas scouring the MEA are the main causes of the accelerated degradation in the front cells of a PEM fuel cell stack under the U-type feed configuration. Several mitigation strategies that would mitigate these phenomena are presented: removing cells that have failed and replacing them with those of the same aging condition as the average of the stack; choosing a Z-type feed pattern instead of a U-type one; putting several air flow-field plates without MEA in the front of the stack; or exchanging the gas inlet and outlet alternately at a certain interval. This paper specifies the causes of the accelerated degradation in the front cells and provides the mitigation strategies.

Key words: Proton exchange membrane fuel cell, Degradation mechanism, Mitigation strategy

1 Introduction

The polymer electrolyte membrane fuel cell(PEMFC) is considered to be one of the most promising candidates as an alternative power system for vehicles due to its high efficiency, low operating temperature, zero or low emissions and fast start-up ability[1–4]. For an automobile powered by PEMFC stack(s), the performance, durability and cost of the whole stack(s) are of greatest concern[5]. However, the performance and reliability of the whole stack(s) depend on the worst performing cell. When the voltage of one cell falls below the critical voltage, failures such as flooding, gas leakage within fuel cells and voltage reversal may occur. These failures can cause irreversible damage to the membrane and catalyst, and subsequently affect the adjacent cells[6]. The required power of the PEMFC stack for an automotive application is quite high, which demands large active area of the membrane electrode assembly(MEA) and a substantial number of fuel cells. Because of the large active area and complicated operations, e.g. quick start-stop and frequent load change, the uniformity of different fuel cells is of great concern, especially in the degradation rate of each cell. When one cell in a PEMFC stack has a higher degradation rate than the others, the load current will be less than expected after a period of operating time. In particular, when the voltage is not uniform, it will accelerate the degradation of the worst cells as well as the adjacent ones. On the contrary, if the degradation rate is uniform, not only can it ensure the stack produces higher power in the long term, but it can also prolong the lifetime of the PEMFC stack and reduce the cost of maintenance.

Normally, every single fuel cell of a stack in a vehicle is monitored and controlled by the cell voltage monitor(CVM). Once the voltage of one cell falls below the warning voltage, the vehicle must be checked to resolve the malfunction. Actually, the real urban road test data of the Tsinghua University fuel cell bus show that the above malfunction is prone to occurring in the front cells of the PEMFC stack. This malfunction severely restricts the running of the vehicle.

Recently, much attention has been paid to the performance degradation of PEMFCs. However, most of this research is focused on the operating condition[7–11] and

* Corresponding author. pchpei@tsinghua.edu.cn
This project is supported by National Basic Research Program of China (973 Program, Grant No. 2012CB215500), National Hi-tech Research and Development Program of China(863 Program, Grant Nos. 2012AA1106012, 2012AA053402), National Natural Science Foundation of China(Grant No. 20976095), and the Specialized Research Fund for the Doctoral Program of Higher Education, China(Grant No. 20090002110074)

internal component failures[12–16]. Other research is concerned with the effect of the configuration of the intake manifold on the pressure and flow distribution in each cell. CHEN, et al[17], built a 2D stack model composed of 72 cells filled with porous media to investigate the flow distribution in the manifold. KOH, et al[18], developed an analytical model to study the pressure and flow distribution in a fuel cell stack manifold. In their research, the pressure variation was mostly influenced by the manifold size and geometry. The non-uniformity of the flow distribution was observed in both U-type and Z-type feed configurations. LEBÆK, et al[19], conducted an experimental study into the pressure and flow distribution in the manifold. They designed a test rig instead of a real fuel cell stack. Their results indicate that the inlet configuration has a great effect on the flow distribution. CHERNYAVSKY, et al[20–21], numerically and experimentally studied the flow turbulence in the manifold. In their study, they designed a pair of headers that consists of inlet and outlet sections connected with a plate containing an array of holes that replicate the unit cells. Using large eddy simulations(LES) and particle image velocimetry(PIV) measurements, they identified that the flow-field and flow structures may have an impact on the overall pressure drop along the header and the effective cross-sectional area of the flow as it leaves the header. However, all these studies are confined only to the pressure and flow distribution; none of them refer to the performance degradation of the fuel cell stack.

In this paper, the intake models of the cathode and anode are built to investigate the flow distribution in the manifold. The flow model results are linked to a single cell model to probe the water content of the membrane(WCM). Based on the experimental and simulation results, four strategies are proposed to mitigate the accelerated degradation in the front cells of a PEMFC stack.

2 Life Time Tests

Considering the configuration of the gas pipes and the other parts of the fuel cell stack system, the U-type and Z-type feed configurations are two common ones adopted in automotive and test bench. Fig. 1(a) shows the U-type feed configuration. The advantage of this type is that the feed pipes are simplified and the stack can be easily installed in a vehicle because the inlets and outlets of the gas, as well as of the coolant, are arranged on the same side. However, the flow path of the reactant gas of the front cells of the stack is shorter than that of the back cells. When the stoichiometry is large, the flux of each cell fluctuates violently. Fig. 1(b) displays the Z-type feed pattern. The flow-field is much more symmetric than that of the U-type feed configuration and the length of the flow path of each cell is basically identical, which leads to very small fluctuation of the incoming gas flux of each cell. Nevertheless, the inlets and outlets are on different sides, which makes it difficult for the stack to be installed because of the limited space available in a vehicle.

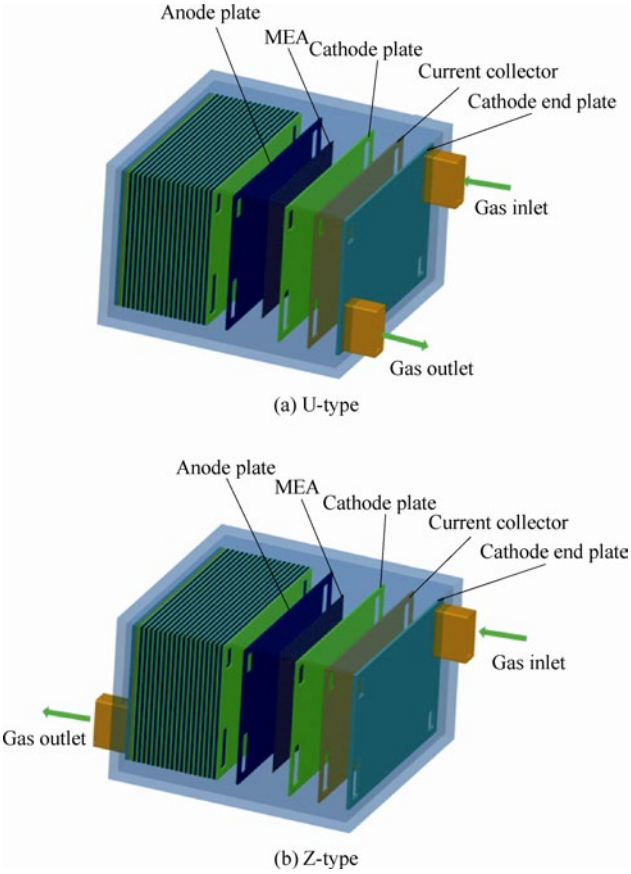

Fig. 1. Different feed configurations

The accelerated degradation tests were done on three different PEMFC stacks(named 1#, 2# and 3#) on the fuel cell accelerated test station(FCATS) manufactured by Greenlight Power Technologies, Inc. Accelerated degradation of the front cells is found in all of them. A description of the test method can be found in references to our group's work[1, 22] and the configurations of our three stacks are listed in Table 1.

Table 1. Configurations of three stacks

Stack	Cell number	Active area/cm^2	Flow-field Layout		Feed pattern
			Anode	Cathode	
1#	100	280	Pin-type	Multiple Serpentine	U
2#	135	280	Straight	Straight	U
3#	80	285	Straight	Multiple Serpentine	U

Fig. 2 shows the average voltage curves of the front 14 cells and subsequent 86 cells of 1# stack before and after the 500 h accelerated test. From Fig. 2, it can be clearly seen that there are discrepancies between performances of the cells after 500 h test. Before the test, the polarization curve of the front 14 cells is similar to that of the subsequent 86 cells, but is even better in the concentration polarization zone(the current density can be up to 800 mA/cm^2). However, after 500 h test the performance of the

front 14 cells decays more rapidly than that of the subsequent 86 cells. Following the test the maximum load current is only 200 mA/cm^2 and the average voltage of the front 14 cells drops 30% at 200 mA/cm^2. Following the test it is also difficult to distinguish activation, ohmic and concentration polarization. The voltage curve drops sharply in the linear zone, which means low activity or severe loss of catalyst, large ohmic impedance of the stack and the membrane with certain damage. Compared with the curve before the test, the performance of the subsequent 86 cells does not drop significantly after the test. At 200 mA/cm^2, the voltage drop is less than 5%. In the activation polarization zone, the curve declines a little. In the ohmic polarization zone, the curve declines slowly. Although the lifetime of the whole PEMFC stack is terminated due to the output power of the stack being unable to reach the requirement for an automobile because of the front 14 cells, the lifetime of the subsequent 86 cells do not cease. Moreover, the operating time(500 h) is less than half of its predicted lifetime deduced from the PEMFC quick lifetime evaluating formula of PEI[22].

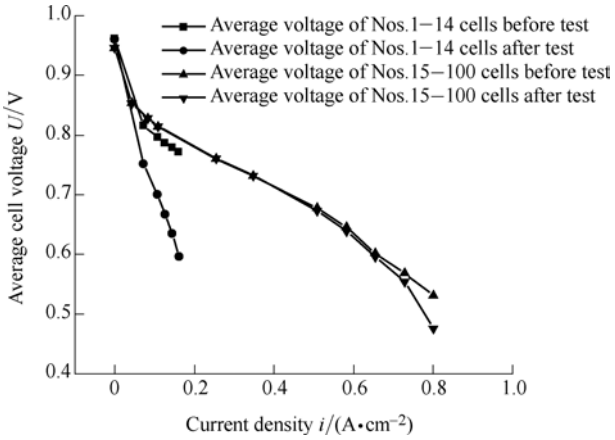

Fig. 2. Polarization curves of 1# stack before and after 500 h test

Fig. 3 shows the voltage variation of every two cells of 1# stack at 200 mA/cm^2 before and after the test(each column stands for the overall voltage of two cells). It can be clearly seen that the voltage of each cell of the stack is consistent before the test. The voltage of each cell is almost the same. The discrepancy between the minimum and maximum voltage is less than 5%. After the test, the voltage of each cell decreases gradually from No. 30 cell to No. 1 cell of the stack against the gas feed direction. From No. 30 cell to No. 100 cell, the voltage of each cell varies a little.

Fig. 4 shows the average voltage curves of the front nine cells and stack before and after the 1 000 h accelerated test. Fig. 5 shows the voltage variation of every three cells of 2# stack at 430 mA/cm^2 before and after the test(each column denotes the overall voltage of three cells). These two figures show the same trends as those of the 1# stack. Although the accelerated degradation in the front cells also exists in the 2# stack, it is less than in the 1# stack. The reason will be explained in the following sections. In general, compared with 1# stack, the maximum load current of 2#stack is still greater after a much longer time test. Compared with Fig. 3, the No. 45 column(the overall voltage of Nos. 133, 134, 135 cells) in Fig. 5 is lower than the adjacent columns after test, which is caused by the cell voltage reversal experiment. This will not be discussed here.

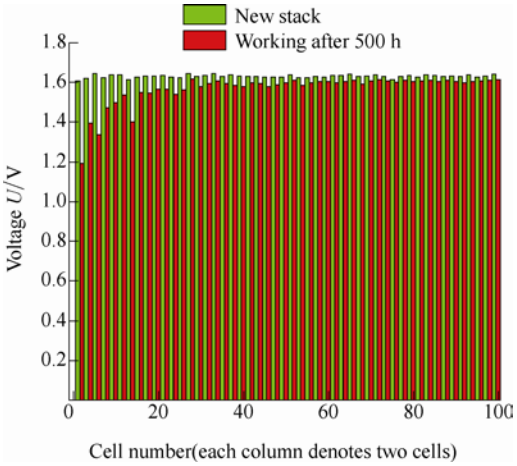

Fig. 3. Cell voltages of 1# stack after 500 h test compared with new stack

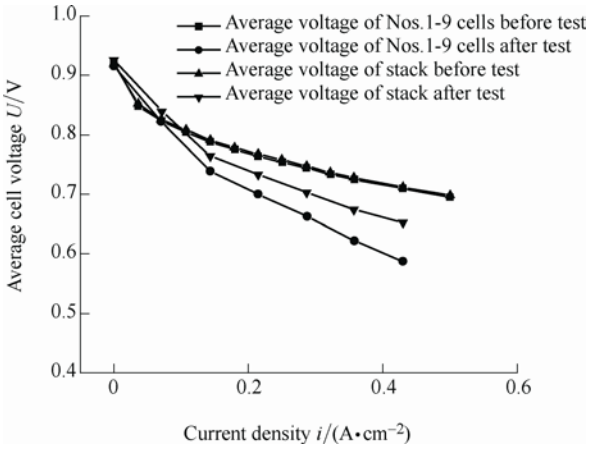

Fig. 4. Polarization curves of 2# stack before and after 1 000 h test

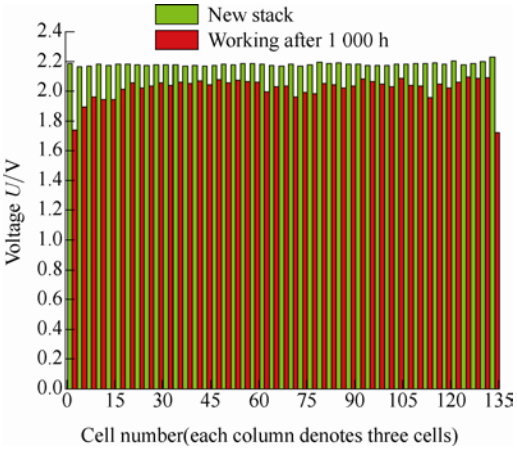

Fig. 5. Cell voltages of 2# stack after 1 000 h test compared with new stack

PEI[23] investigated the front 8 cells of 1# stack and found that compared with the back cells of the stack the performance of the front ones was much worse, whichever criterion was selected: smaller active area; more catalyst particle agglomeration; higher ohmic impedance or lower voltage at the same current density. The MEA test showed that the content of the catalyst dropped considerably and that the cells produced water that was weakly acidic, indicating the presence of Hydrogen Fluoride(HF) as a consequence of severe damage to the membrane.

The accelerated degradation in the front cells of a stack, which occurs in the 1# and 2# stack, is also found in the PEMFC stack of the Tsinghua University fuel cell bus. In order to find out why the performance of the fuel cells close to the gas inlet decays faster, an investigation of the working conditions of each cell is required.

3 Numerical Simulation

3.1 Model description

As mentioned above, the accelerated degradation in the front cells occurs in two stacks that have different cell numbers and flow-field configurations but the same feed patterns. This means the feed patterns may have an important impact. In this section, 2# stack will be taken as an example to illustrate the effect of feed patterns on the accelerated degradation in the front cells. The whole stack model and the unit cell model of 2# stack are built to investigate the WCM and the gas intake velocity. The experimental data of 2# stack is based on the U-type feed configuration.

To simplify the computation and to reduce computation time, the computing process is divided into two steps. In the first step, models of the whole stack of the cathode and anode flow-field respectively are built. We do not consider the electrochemical reaction here, rather calculate the incoming flux and exit pressure of each unit cell. In the second step, the model of a unit cell is built. By importing the results of the first step, the WCM of each cell can be investigated.

In the first step, the following assumptions are made.

(1) Steady and incompressible flows.

(2) Isothermal condition(333 K).

(3) Only species transport is considered.

(4) There is no liquid water, with all water vapor produced on the cathode side.

(5) The reactions in the MEA is homogeneous, consequently the consumption of the oxygen and hydrogen as well as the production of the water vapor in the MEA are also homogeneous.

(6) For both sides(anode and cathode), we neglect the diffusion process; instead we assume that hydrogen "flow" in or out from the interface of the flow channel and MEA.

The second assumption is plausible for the following reason. The operating current density that is chosen in the simulation is not large(500 $\mathrm{mA/cm^2}$), which means relatively little enthalpy of reaction will be created. The 2# stack in the test bench is cooled by water, and the coolant temperature of inlet and outlet are respectively 60 and 63 ℃. Therefore, the stack can be considered to be approximately isothermal.

The flow in the manifold is considered turbulent. In order to model the turbulent flow, the k-ε model is employed to solve the related transport equations. The governing equations are listed as below.

Mass conservation:

$$\nabla \cdot \boldsymbol{V} = 0 . \tag{1}$$

Momentum equation:

$$\nabla \cdot (\rho \boldsymbol{V}\boldsymbol{V}) = -\nabla P + \nabla \cdot (\boldsymbol{\tau}), \tag{2}$$

$$\boldsymbol{\tau} = \mu \left[\left(\nabla \boldsymbol{V} + \nabla \boldsymbol{V}^{\mathrm{T}} \right) - \frac{2}{3} \nabla \cdot \boldsymbol{V} \boldsymbol{T} \right], \tag{3}$$

where $\boldsymbol{\tau}$ is the stress tensor, μ is the viscosity, and $\boldsymbol{T}$ is the unit tensor.

Turbulent kinetic energy(k) equation:

$$\frac{\partial (\rho k V_i)}{\partial x_i} = \frac{\partial}{\partial x_j} \left[\left(\mu + \frac{\mu_{\mathrm{t}}}{\sigma_k} \right) \frac{\partial k}{\partial x_j} \right] + G_k - \rho \varepsilon . \tag{4}$$

Turbulent dissipation rate(ε) equation:

$$\frac{\partial (\rho \varepsilon V_i)}{\partial x_i} = \frac{\partial}{\partial x_j} \left[\left(\mu + \frac{\mu_{\mathrm{t}}}{\sigma_\varepsilon} \right) \frac{\partial \varepsilon}{\partial x_j} \right] + C_{1\varepsilon} G_k \frac{\varepsilon}{k} - C_{2\varepsilon} \rho \frac{\varepsilon^2}{k}, \tag{5}$$

where k and ε are the turbulent kinetic energy and dissipation rate respectively. μ_{t} is the turbulent viscosity and is computed as follows:

$$\mu_{\mathrm{t}} = \rho C_\mu \frac{k^2}{\varepsilon} . \tag{6}$$

G_k is a measure of the production of the turbulent kinetic energy and defined as

$$G_k = -\rho \overline{V_i' V_j'} \frac{\partial V_j}{\partial x_i}, \tag{7}$$

σ_k=1.0, σ_ε=1.3, $C_{1\varepsilon}$=1.44, $C_{2\varepsilon}$=1.92, C_μ=0.09 are the empirical constants.

For the anode side, the inlet mass flow rates and outlet pressure are obtained from experimental data. For the cathode side, the inlet mass flow rate is updated by subtracting the reacting oxygen. The velocity of hydrogen "flowing" into and out of the interface of the flow channels and MEA is decided by the following:

$$V_H = \frac{Q_H}{\rho_H A_i}, \tag{8}$$

$$Q_H = k_e^H I, \tag{9}$$

where Q_H is the mass flow rate of consuming hydrogen, A_i is the area of the interface of the flow channels and MEA, k_e^H is the hydrogen electrochemical equivalent, and I is the load current.

In the second step, the calculated results including the mass flow rate and exit pressure from the first step are used as the boundary conditions of the unit cell model. Three sub-models, respectively electrochemistry sources, Butler-Volmer rate and membrane water transport, were chosen in this work. The simulation was conducted using the commercial code ANSYS Fluent-Fuel Cell model. Model equations and detailed information of this software for fuel cell simulation can be found in LI's[24] work and the Fluent user manual provided by ANSYS, Inc.

As mentioned in Table 1, the flow-field pattern of anode and cathode of 2# stack are both straight. Fig. 6 depicts the cathode flow-field and unit cell geometry. The operating and geometry parameters are listed in Table 2.

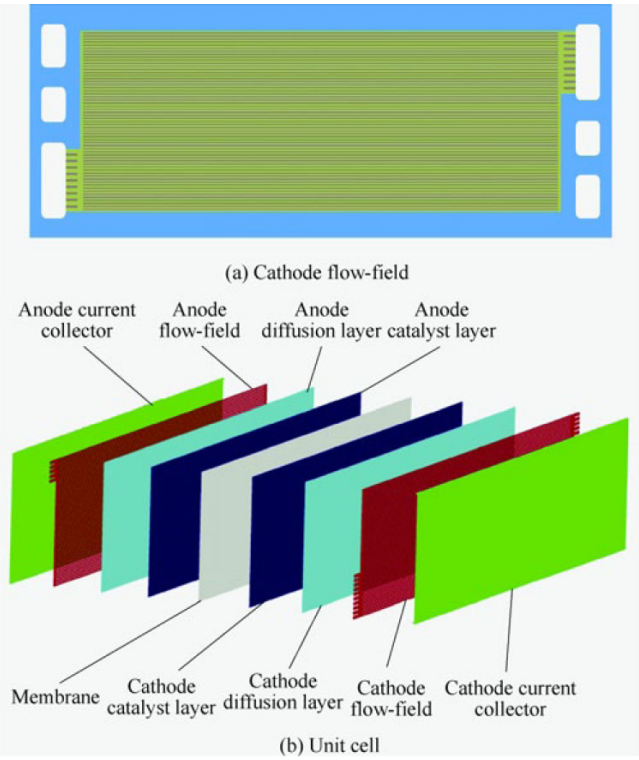

Fig. 6. Second step model geometry

3.2 Simulation results and discussion

Fig. 7 shows the comparison between two feed patterns in terms of mass flow rate, pressure drop and the incoming gas velocity on the cathode side of each cell. From Fig. 7, it can be seen that the mass flow rate, pressure drop and incoming gas velocity of the cathode of each cell under the U-type feed pattern decrease from the inlet to the outlet. For example the mass flow rate, pressure drop and incoming gas velocity of No. 1 cell under the U-type feed pattern are 13.1%, 16.7%, 320% larger than those of No. 135, respectively. The gas flow path of the front cells is shorter than that of the back and the resistance to air flow in the front cells is smaller. Consequently most of the air enters the front cells. The average magnitude of the incoming gas velocity in the front ten cells is about 30 m/s, which means that the catalyst of the front cells is prone to being scoured. In the PEMFC working process, most of water is generated in cathode side and the partial pressure of oxygen in air is only 21%. In order to provide sufficient oxygen and to remove water so as to avoid flooding the electrode and blocking the flow channels, a relatively large stoichiometry of air is adopted(usually>2). On the cathode side during transient operation gas starvation shows a

Table 2. Parameters of the simulation

Parameter	Value
Cathode channel width $C_{w,c}$/mm	0.8
Cathode channel depth $C_{d,c}$/mm	0.8
Anode channel width $C_{w,a}$/mm	0.8
Anode channel depth $C_{d,a}$/mm	0.6
Cathode rib width $C_{l,c}$/mm	0.6
Anode rib width $C_{l,a}$/mm	0.6
Cathode plate thickness $\delta_{pl,c}$/mm	1.6
Anode plate thickness $\delta_{pl,a}$/mm	1.0
Cathode diffusion layer thickness $\delta_{diff,c}$/μm	200
Anode diffusion layer thickness $\delta_{diff,a}$/μm	200
Cathode/anode catalyst layer thickness $\delta_{cata,c}$/μm	15
Anode catalyst layer thickness $\delta_{cata,a}$/μm	10
PEM thickness δ_{mem} /μm	50
Active area A/cm^2	280
Cathode diffusion layer porosity $\varepsilon_{diff,c}$	0.5
Anode diffusion layer porosity $\varepsilon_{diff,a}$	0.4
Cathode catalyst layer porosity $\varepsilon_{cata,c}$	0.5
Anode catalyst layer porosity $\varepsilon_{cata,a}$	0.4
PEM porosity ε_{mem}	0.28
Cathode diffusion layer permeability $K_{diff,c}$/m^2	3.0×10^{-13}
Anode diffusion layer permeability $K_{diff,a}$/m^2	3.0×10^{-13}
Cathode catalyst layer permeability $K_{cata,c}$/m^2	3.0×10^{-13}
Anode catalyst layer permeability $K_{cata,c}$/m^2	3.0×10^{-13}
PEM permeability K_{mem}/m^2	1.8×10^{-18}
Diffusion layer electric conductivity D_{diff}/(S • m^{-1})	570
Catalyst layer electric conductivity D_{cata}/(S • m^{-1})	570
Bipolar plate electric conductivity D_{pl}/(S • m^{-1})	3 703
PEM ionic conductivity ζ	Springer model[25]
Cathode reference current density $i_{ref,c}$/(A • m^{-3})	1.05×10^{6}
Anode reference current density $i_{ref,a}$/(A • m^{-3})	9.23×10^{8}
Transfer coefficient at cathode β_c	1.5
Transfer coefficient at anode β_a	0.5
O_2 concentration dependence γ_c	1.0
H_2 concentration dependence γ_a	0.5
Open circuit voltage V_o/V	0.95
Temperature T/K	333
Operating current density i/(mA • cm^{-2})	600
Air inlet pressure $P_{in,c}$/kPa	140
H_2 inlet pressure $P_{in,a}$/kPa	110
Air stoichiometry λ_c	2.5
H_2 stoichiometry λ_a	1.2
Air inlet RH RH_c	50%
H_2 inlet RH RH_a	100%

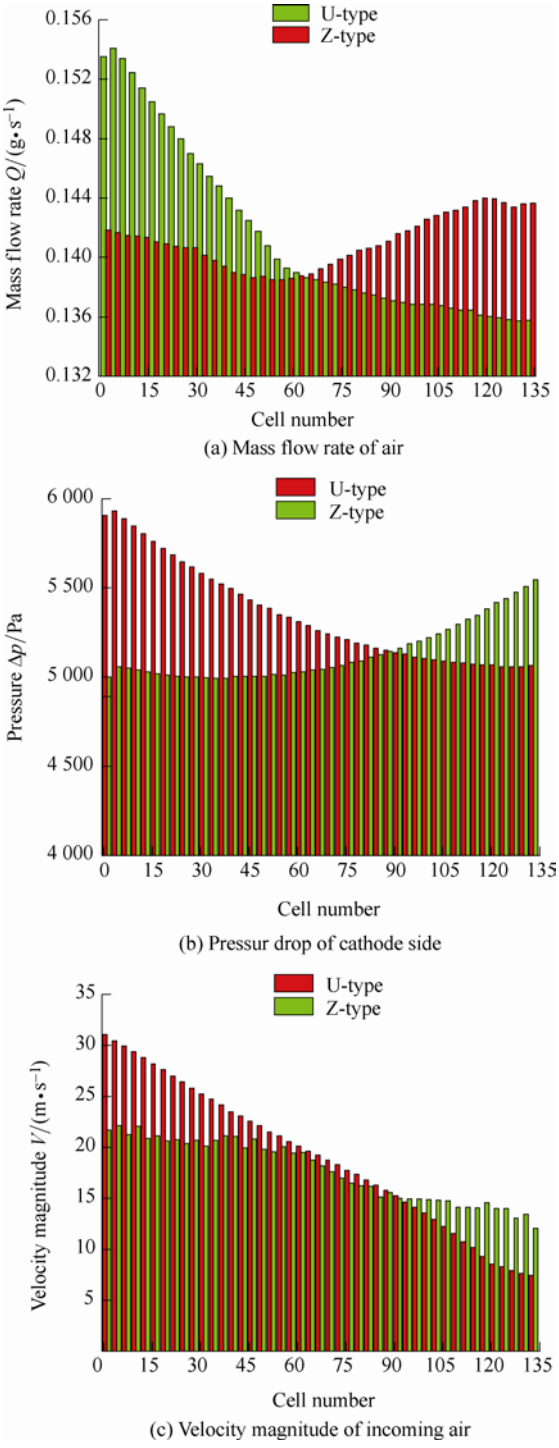

Fig. 7. Comparisons of two feed patterns at the operation current density 600 mA/cm^2

particular tendency to occur, which means a much larger stoichiometry is required. However, a larger air stoichiometry implies a higher velocity of incoming air to the fuel cells close to the inlet of the PEMFC stack. With the consequent high-speed air scouring, it will exacerbate the loss of catalyst and the dissolution of the membrane. The performance of the front cells will drop severely at certain times and will not recover to the original level. This results in a reduction in the lifetime of the PEMFC stack. In contrast to the U-type feed pattern, the mass flow rate, pressure drop and incoming gas velocity of each cell under the Z-type feed pattern, demonstrate a lower variance. The maximum of the mass flow rate of single cell is only 3.97% larger than the minimum. At the same time, the magnitude of the incoming gas flow in No. 1 cell decreases by 32.5% compared with that under the U-type feed pattern.

The WCM is very important for the performance of PEMFC. It determines the proton conduction rate and the ohmic impedance of the membrane. If the WCM is bigger, the proton conduction rate of membrane is higher and the ohmic impedance is lower. Moreover, if the membrane is always in a dehydrated state, an accelerated degradation of fuel cell will occur. Fig. 8 shows the WCM under two feed configurations at the operating current density of 600 mA/cm^2. It can be seen that the WCM in the front cells under the U-type feed configuration is lower than that of the back cells. The WCM of No. 1 cell is 12% less than that of No. 135 cell. When the cell number is bigger than 11, variance in WCM diminishes. The mass flow rates of the front cells are larger than those of the back cells and the inlet relative humidity of air(50%) is less than that of hydrogen(100%). Consequently more water will be transported from the membrane to the cathode channel in the front cells due to the concentration gradient. Hence, the WCM value for the front cells under the U-type feed pattern decreases. For the Z-type feed configuration, the WCM variance is small. The standard deviation of WCM across all cells is only 0.032. This means that the membrane in the front cells under the Z-type feed configuration is likely to remain hydrated.

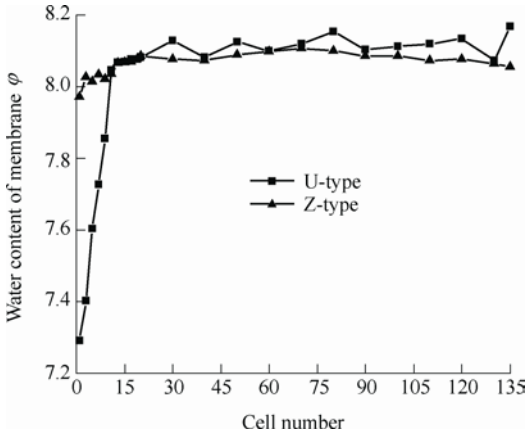

Fig. 8. Water content of membrane under two feed patterns

4 Mitigation Strategies

The accelerated degradation in the front cells is an obstacle to improving the reliability and lifetime of the PEMFC stacks for automotive applications. Based on the above study, the reasons the front cells in a stack have a larger degradation rate are respectively the dry condition of the membranes near the gas inlet and the effect of high-speed gas scouring of the MEA. To mitigate this phenomenon, four strategies are proposed.

4.1 Strategy I

Even if the whole stack cannot be loaded at the expected current due to a number of faulty cells, the majority of cells can still work. If the lifetime of the whole PEMFC stack is regarded as being terminated because a small number of cells failed to work, it will increase the cost significantly. If we remove or replace the fault cells with those of the same aging condition as the average, the stack can still work normally.

Fig. 9 shows the voltage variation with time of different cells of 1# stack. The test current in Fig. 9 was only 50 A because the load current could not be sustained at 100 A after 240 h. The performance of No. 1-No. 4 fuel cells was not stable and declined sharply after 240 h. However, at the same time the cells in the middle and back of the stack worked normally. After another 140 h test, the front 14 cells were replaced with new ones. It was found that the performance of all cells of the new 1# stack had fine uniformity and was even better than that before replacement. This indicates that replacement with new cells mitigates the effects of accelerated degradation of the front cells and prolongs the lifetime of the stack.

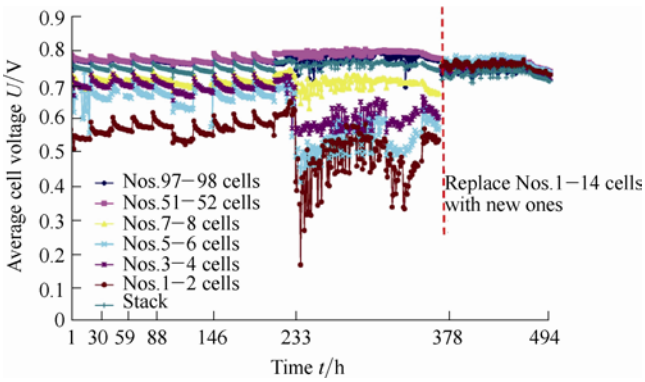

Fig. 9. Voltage variation of 1# stack by removing failure cells

The 3#stack originally had 80 fuel cells. After more than 300 h test, the front two fuel cells failed to work and were removed. The remaining 78 fuel cells were assembled to a new 3#stack. From Fig. 10 it can be seen that the performance of the new 3# stack did not drop sharply and the decaying rate remained the same as the original 3# stack. But after another 200 h test, the two front cells of the new 3# stack(the original No. 3 and No. 4 cells) failed to work due to the effect of the accelerated degradation in the front cells of a stack. They were then replaced. Fig. 10 demonstrates that the performance of the two new cells was much better than the other 76 cells. However, after replacing the two fault cells the degradation rate of the other 76 cells was a little bit larger than that of before the replacement.

The test results reveals that within a certain time period the performance of the whole stack can re-main stable by removing or replacing the faulty fuel cells with new ones and it is an effective method of mitigating the accelerated degradation in the front cells. However, replacing the faulty fuel cells with new ones may exacerbate the degradation of the original cells. If, after consideration the replacement of the faulty cells is necessary, we strongly suggested using cells of the same aging condition equivalent to the stack average.

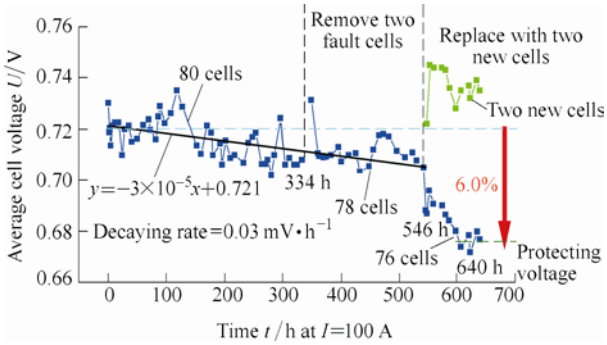

Fig. 10. Voltage variation of 3# stack by removing and replacing failure cells with new ones

4.2 Strategy II

According the description of section 3, the incoming gas velocity and WCM of each cell were calculated. Through the computation results, it can be concluded that (i) the WCM of the fuel cells close to the inlet of the Z-type feed configuration is more than that of the U-type feed configuration, and (ii) the effect of the gas scouring effect on the membrane and catalyst of the Z-type feed configuration is reduced under the same operating condition. Therefore, if the space is available, we can change the U-type to the Z-type feed configuration to avoid the membrane working under dry conditions. In this way, we can prolong the lifetime of the PEMFC stack and save cost.

4.3 Strategy III

Fig. 11 shows a schematic of where several air flow-field plates without MEA are assembled ahead of the cathode current collector. These additional cathode plates simply direct the air flow but do not generate electricity. Comparing Fig. 2 and Fig. 3 with Fig. 4 and Fig. 5, although there is an accelerated degradation in the front cells existing in 1# and 2# stack, the phenomenon of 2# stack is less. One important reason is that several air plates without MEA were put ahead of the cathode current collector in 2# stack but not in 1# stack. The distribution of the incoming gas flow and pressure can be altered by this means. This modification will also decrease the velocity of the incoming gas of the front cells. Consequently, the WCM of the front cells increases and the effect of gas scouring on the membrane and catalyst integrity is reduced. However, the efficiency of the whole stack is reduced and the volume of the stack becomes larger due to the additional, non-generating plates.

4.4 Strategy IV

Fig. 12 presents the schematic of a reconfiguration scheme for the gas inlet and outlet of a PEMFC stack. With regard to the phenomenon that the fuel cells close to the gas

inlet work under dry condition while the fuel cells close to gas outlet work under 'flooding' condition due to the byproduct water accumulation downstream, the gas inlet and outlet can be exchanged at a certain interval to avoid the above phenomenon. As shown in Fig. 12, the valves 1, 3 are initially open while valves 2, 4 are closed. After a period of operating time(e.g. 10 min), the membranes near the inlet are dehydrated while the membranes near the outlet are working under flooding condition, the flow direction of the reactant gas is then reversed by opening valves 2, 4 and closing valves 1, 3. Thus, the dehydrated membranes near the original inlet can be supplied with sufficient water and the excess water of membranes near the original outlet will be removed. This strategy can ensure that the membranes of the stack are hydrated. Nevertheless, it cannot mitigate the effect of high speed gas scouring the membranes near the inlet.

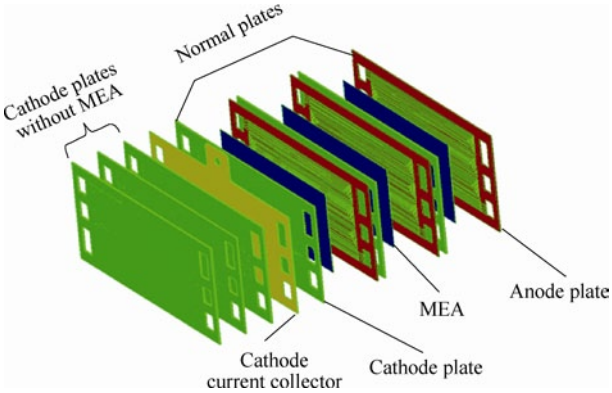

Fig. 11. Schematic of several air plates without MEA ahead of the stack

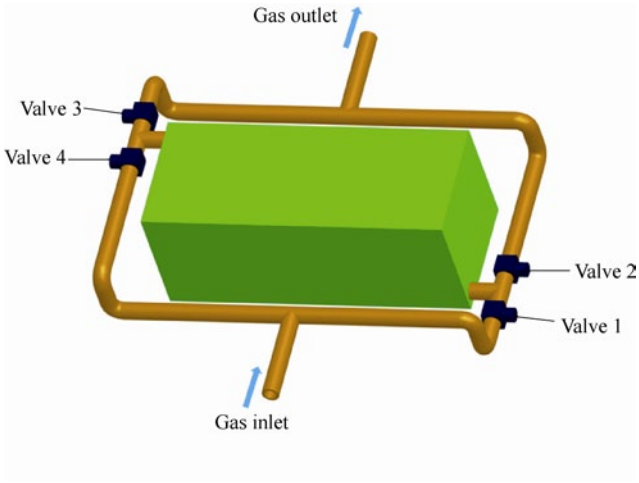

Fig. 12. Schematic of exchanging the gas inlet and outlet of a PEMFC stack at a certain interval

5 Conclusions

(1) When the fuel cell stack is under the U-type feed configuration, the mass flow rate and the pressure drop of the front cells are larger than those of the back cells, making the intake gas velocity quite high. The high-speed flow of gas may scour the MEA, leading to the loss of catalyst and degradation of the membrane. Moreover, the flow maldistribution results in lower WCM of the front cells, which can degrade the proton conductivity and the performance of the stack. These two issues are the main causes of the accelerated degradation in the front cells.

(2) Based on the experimental and simulated data, four strategies are proposed to mitigate the accelerated degradation in the front cells, namely (i) removing cells that have failed and replacing them with those of the same aging condition as the average of the stack; (ii) choosing a Z-type feed pattern instead of a U-type one; (iii) putting several air flow-field plates without MEA in the front of the stack or (iv) exchanging the gas inlet and outlet alternately at a certain interval. These strategies can be applied to all PEMFC stacks individually or in combination to achieve an improved performance and extended life for the stack.

Acknowledgements

The authors are grateful to Prof. STOBART Richard, *Loughborough University, UK*, for his help in revising the manuscript.

References

[1] PEI Pucheng, YUAN Xing, LI Pengcheng, et al. Lifetime evaluating and the effects of operation conditions on automotive fuel cells[J]. *Chinese Journal of Mechanical Engineering,* 2010, 23(1): 66–71.

[2] LIN Rui, ZHAO Tiantian, ZHANG Haiyan, et al. Influence of PTFE on electrode structure for performance of PEMFC and 10-cells stack[J]. *Chinese Journal of Mechanical Engineering,* 2012, 25(6): 1 171–1 175.

[3] MEIDANSHAHI V, KARIMI G. Dynamic modeling, optimization and control of power density in a PEM fuel cell[J]. *Applied Energy*, 2012, 93: 98–105.

[4] OBAYOPO S O, BELLO-OCHENDE T, MEYER J P. Modelling and optimization of reactant gas transport in a PEM fuel cell with a transverse pin fin insert in channel flow[J]. *International Journal of Hydrogen Energy*, 2012, 37(13): 10 286–10 298.

[5] LI Bing, LI Hui, MA Jianxin, et al. PEM fuel cells: current status and challenges for electrical vehicle applications[J]. *Journal of Automotive Safety and Energy,* 2010, 1(4): 260–269.

[6] ZHANG Fengyuan, ADVANI S G, PRASAD A K, et al. Quantitative characterization of catalyst layer degradation in PEM fuel cells by X-ray photoelectron spectroscopy[J]. *Electrochimica Acta,* 2009, 54(16): 4 025–4 030.

[7] YOUSFI-STEINER N, MOÇOTÉGUY P, CANDUSSO D, et al. A review on PEM voltage degradation associated with water management: Impacts, influent factors and characterization[J]. *Journal of Power Sources,* 2008, 183(1): 260–274.

[8] O'ROURKE J, RAMANI M, ARCAK M. In situ detection of anode flooding of a PEM fuel cell[J]. *International Journal of Hydrogen Energy*, 2009, 34: 6 765–6 760.

[9] HOU Junbo, YU Hongmei, YANG Min, et al. Reversible performance loss induced by sequential failed cold start of PEM fuel cells[J]. *International Journal of Hydrogen Energy,* 2011, 36(19): 12 444–12 451.

[10] FOWLER M W, MANN R F, AMPHLETT J C, et al. Incorporation of voltage degradation into a generalized steady state

electrochemical model for a PEM fuel cell[J]. *Journal of Power Sources*, 2002; 106(1–2): 274–283.

[11] ANDREASEN S J, VANG J R, KÆR S K. High temperature PEM fuel cell performance characterisation with CO and CO_2 using electrochemical impedance spectroscopy[J]. *International Journal of Hydrogen Energy*, 2011, 36(16): 9 815–9 830.

[12] TANG Haolin, SHEN Peikang, JIANG Sanping, et al. A degradation study of Nafion proton exchange membrane of PEM fuel cells[J]. *Journal of Power Sources*, 2007, 170(1): 85–92.

[13] ZHANG Shengsheng, YUAN Xiaozi, WANG Haijiang, et al. A review of accelerated stress tests of MEA durability in PEM fuel cells[J]. *International Journal of Hydrogen Energy*, 2009, 34(1): 388–404.

[14] SEO Dongho, LEE Junghyun, PARK Sangsun, et al. Investigation of MEA degradation in PEM fuel cell by on/off cyclic operation under different humid conditions[J]. *International Journal of Hydrogen Energy*, 2011, 36(2): 1 828–1 836.

[15] LIN R, LI B, HOU Y P, et al. Investigation of dynamic driving cycle effect on performance degradation and micro-structure change of PEM fuel cell[J]. *International Journal of Hydrogen Energy*, 2009, 34(5): 2 369–2 376.

[16] WU Bi, FULLER T F. Modeling of PEM fuel cell Pt/C catalyst degradation[J]. *Journal of Power Sources*, 2008, 178(1): 188–196.

[17] CHEN Chunghsien, JUNG Shiauhping, YEN Shichern. Flow distribution in the manifold of PEM fuel cell stack[J]. *Journal of Power Sources*, 2007, 173(1): 249–263.

[18] KOH J, SEO H, LEE C, et al. Pressure and flow distribution in internal gas manifolds of a fuel-cell stack[J]. *Journal of Power Sources*, 2003, 115(1): 54–65.

[19] LEBÆK J, BANG M, KÆR S K. Flow and pressure distribution in fuel cell manifolds[J]. *Journal of Fuel Cell Science and Technology*, 2010, 7: 061 001–061 008.

[20] CHERNYAVSKY B, SUI P C, JOU B S, et al. Turbulent flow in the distribution header of a PEM fuel cell stack[J]. *International Journal of Hydrogen Energy*, 2011, 36(12): 7 136–7 151.

[21] CHERNYAVSKY B, RAVI K, SUI P C, et al. Numerical investigation of flowfield in PEM fuel cell stack headers[J]. *Energy Procedia*, 2012, 29: 102–111.

[22] PEI Pucheng, CHANG Qianfei, TANG Tian. A quick evaluating method for automotive fuel cell lifetime[J]. *International Journal of Hydrogen Energy*, 2008, 33(14):3 829–3 836.

[23] PEI Pucheng, YUAN Xing, CHAO Pengxiang, et al. Analysis on the PEM fuel cells after accelerated life experiment[J]. *International Journal of Hydrogen Energy*, 2010, 35(7): 3 147–3 151.

[24] LI Shaoping, BECKER U. A three dimensional CFD model for PEMFC[C]// *2nd International Conference on Fuel Cell Science, Engineering and Technology*, New York, USA, June 14–16, 2004: 157–164.

[25] SPRINGER T E, ZAWODINSKI T A, GOTTESFELD S. Polymer electrolyte fuel cell model. *Journal of the Electrochemical Society*, 1991, 138: 2 334–2 342.

Biographical notes

LI Pengcheng, born in 1981, is currently a PhD candidate at *School of Transportation Science and Engineering, Beihang University, China*. He received his bachelor degree from *Beihang University, China*, in 2004. His research interests include fuel cell design and computational fluid dynamics.
Tel: +86-10-82311431; E-mail: iamlpc@ae.buaa.edu.cn

PEI Pucheng, born in 1965, is currently a professor at *State Key Laboratory of Automotive Safety and Energy, Tsinghua University, China*. His research interests include lifetime evaluation of automotive fuel cell and engine electronic control.
Tel: +86-10-62788558; E-mail: pchpei@tsinghua.edu.cn

HE Yongling, born in 1963 is currently a professor at *School of Transportation Science and Engineering, Beihang University, China.* His research interests include engine design and electronic control.
Tel: +86-10-82339869; E-mail: xkbhe@buaa.edu.cn

YUAN Xing, born in 1982, is a doctor at *State Key Laboratory of Automotive Safety and Energy, Tsinghua University, China.*
E-mail: yuanx@mails.tsinghua.edu.cn

CHAO Pengxiang, born in 1985, is a master at *State Key Laboratory of Automotive Safety and Energy, Tsinghua University, China.*
E-mail: cpx07@mails.tsinghua.edu.cn

WANG Xizhong, born in 1968, is a laboratory assistant at *State Key Laboratory of Automotive Safety and Energy, Tsinghua University, China*. She received her B E degree in thermal power engineering from *Northwestern Polytechnical University* in 1989
E-mail: morning_bell@263.net